

Cite this: *Chem. Commun.*, 2018, 54, 2349Received 26th December 2017,  
Accepted 5th February 2018

DOI: 10.1039/c7cc09866a

rsc.li/chemcomm

## Highly photoluminescent two-dimensional imine-based covalent organic frameworks for chemical sensing†

 Qiang Gao,<sup>a</sup> Xing Li,<sup>b</sup> Guo-Hong Ning,<sup>b</sup> Kai Leng,<sup>b</sup> Bingbing Tian,<sup>a</sup> Cuibo Liu,<sup>ab</sup> Wei Tang,<sup>c</sup> Hai-Sen Xu<sup>b</sup> and Kian Ping Loh<sup>ab\*</sup>

The strong  $\pi$ - $\pi$  interactions in the stacking layers of two-dimensional covalent organic frameworks (2D-COFs), together with rotationally labile imine linkages, make most of the solid state imine-linked COFs non-fluorescent due to fluorescence quenching processes. Here, we report the successful synthesis of highly photoluminescent imine-based 2D-COFs by integrating a non-planar building unit with a pyrene-based unit and transforming the COF into spherical, sub-micron particles. High photoluminescence quantum yields (PLQY) were achieved with COF sub-micron particles dispersed in organic solvents. The as-prepared COF sub-micron particles can be used as a chemical sensor for the detection of explosive chemicals, with high sensitivity and selectivity (up to ppm level).

Covalent organic frameworks (COFs) are an emerging class of ordered conjugated organic polymer materials constructed through the covalent linkages of organic building blocks *via* reversible bond formation chemistry.<sup>1</sup> Enjoying the advantages of low densities, high surface areas and thermal stabilities, COFs show broad applications in gas storage,<sup>2</sup> heterogeneous catalysis,<sup>3</sup> chemical sensors,<sup>4</sup> drug delivery,<sup>5</sup> energy conversion and storage<sup>6</sup> *etc.* In general, 2D-COFs are assembled *via*  $\pi$ - $\pi$  stacking interactions, thus the aggregation-caused quenching (ACQ) effect results in non- or less-emissive 2D-COFs. Highly emissive 2D-COFs based on fluorescent pyrene and aggregation-induced emission (AIE) building units had been reported using the boronate ester linkage<sup>4b</sup> and azine-linkage.<sup>4a</sup> However most of the imine-linked 2D-COFs reported previously were non- or weakly fluorescent.<sup>7</sup> To prevent fluorescence quenching

by strong  $\pi$ - $\pi$  stacking interactions, Wang *et al.* demonstrated a pyrene-based fluorescent 3D imine COF (3D-Py-COF).<sup>4g</sup> Apart from the 3D bonding framework, the synthesis of highly photoluminescent 2D-COFs linked by imine bonds remains a challenge.

To achieve highly emissive 2D-COFs, Jiang *et al.* designed a boronate ester based 2D-COF consisting of an aggregation-induced emission (AIE) moiety (TPE-Ph COF).<sup>4b</sup> Imine COFs, with higher stability and easier chemical conversion,<sup>8</sup> are more suited than boronate ester-linked COFs for applications in catalysis, gas adsorption and chemical sensors. Although strong photoluminescence can be seen in boronate ester-linked COFs, there has been no photoluminescent tetraphenylethene (TPE)-based imine COFs reported thus far. Herein, we develop a general strategy for constructing a highly luminescent imine-based 2D-COF based on the integration of a non-planar TPE building unit with a pyrene unit (Fig. 1), and engineering the morphology of the COF into spherical, sub-micron sized particles. High photoluminescent quantum yield (up to 21.1%) is achieved from COF nanoparticles that are dispersed in organic solvents. Furthermore, our pyrene-TPE-based imine 2D-COF (Py-TPE-COF) nanoparticles can be used to sense explosive chemicals with high sensitivity and selectivity (up to ppm level).

To construct our Py-TPE-COF, 1,3,6,8-tetrakis(4-aminophenyl)pyrene (**1**) is chosen as the amine unit because of the fluorescence properties of the pyrene motif. Due to the topology and assembly rules of building blocks, the non-planar 1,1,2,2-tetrakis(4-formylphenyl)ethane (TPE-4CHO, **2**), with the function of AIE, is selected as the aldehyde unit. To our delight, a highly crystalline Py-TPE-COF has been successfully synthesized *via* [4+4] imine condensation under solvothermal conditions (ESI†). To confirm the formation of the imine bond linkage in the Py-TPE-COF, Fourier transform infrared spectroscopy (FT-IR) and solid state <sup>13</sup>C CP-MAS NMR characterization were performed. The FT-IR spectrum of the Py-TPE-COF shows the stretching vibration band of the imine bond (C=N) at 1622 cm<sup>-1</sup>, while model compounds Py-M and TPE-M (Fig. S1, ESI†) also display the similar C=N vibration bands at 1625 cm<sup>-1</sup> and 1624 cm<sup>-1</sup>, respectively (Fig. S10, ESI†). Solid state <sup>13</sup>C CP-MAS NMR

<sup>a</sup> SZU-NUS Collaborative Innovation Center for Optoelectronic Science & Technology, Key Laboratory of Optoelectronic Devices and Systems of Ministry of Education and Guangdong Province, College of Optoelectronic Engineering, Shenzhen University, Shenzhen 518060, China

<sup>b</sup> Department of Chemistry, Centre for Advanced 2D Materials (CA2DM), National University of Singapore, 3 Science Drive 3, Singapore 117543, Singapore

<sup>c</sup> Institute of Materials Research and Engineering, A\*STAR, 2 Fusionopolis Way, Innovis, Singapore 138634, Singapore. E-mail: chmlhkp@nus.edu.sg

† Electronic supplementary information (ESI) available. See DOI: 10.1039/c7cc09866a

‡ These authors contributed equally to this work.

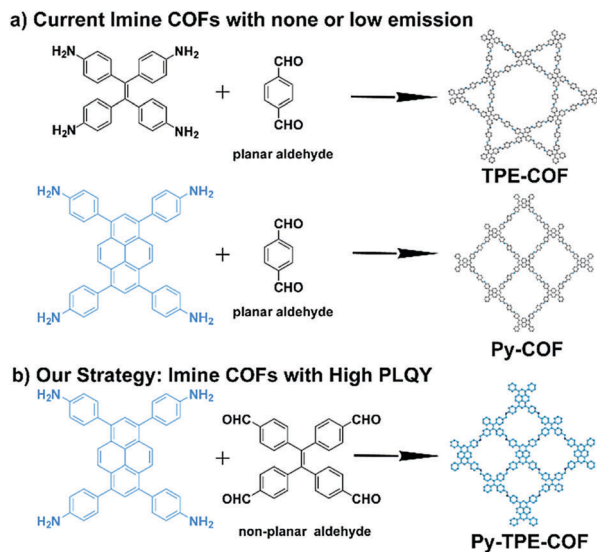


Fig. 1 Strategies for constructing imine-based 2D-COFs with high photoluminescence quantum yield (PLQY).

spectroscopy of the Py-TPE-COF reveals a characteristic resonance signal at 157.4 ppm, further confirming the presence of C=N imine bonds (Fig. S8, ESI<sup>†</sup>). In addition, thermal gravimetric analysis (TGA) shows that the Py-TPE-COF is thermally stable under a nitrogen atmosphere (up to 400 °C, Fig. S9, ESI<sup>†</sup>). Elemental analysis of the Py-TPE-COF reveals that the contents of carbon, hydrogen, and nitrogen of the COF are 87.24%, 4.30%, and 5.81%, respectively, which are close to the theoretically calculated values (89.53% for C, 4.51% for H, and 5.97% for N).

The crystallinity of the Py-TPE-COF is determined by powder X-ray diffraction (PXRD) analyses using Cu K $\alpha$  radiation (Fig. 2 and Fig. S3, ESI<sup>†</sup>). The observed PXRD patterns of the Py-TPE-COF exhibit PXRD peaks at 5.85°, 8.56°, 11.67°, 13.42°, 17.40° and 19.53°, which could be assigned to the (220), (400), (440), (260), (660), and (001) planes, respectively (Fig. 2a). To further determine the crystal structure of the Py-TPE-COF, theoretical simulations are carried out using Materials Studio (version 2016, ESI<sup>†</sup>). Unit cell parameters of  $a = 42.63$  Å,  $b = 43.72$  Å,  $c = 4.57$  Å,  $\alpha = \gamma = 90^\circ$ , and  $\beta = 78.8^\circ$  with the  $C2/m$  space group are obtained through geometry and energy minimization (Table S1 and Fig. S26–S29, ESI<sup>†</sup>). The simulated PXRD patterns of the eclipsed structure show very good agreement with the experimental PXRD patterns, either in peak positions or in relative intensities (Fig. 2b and d). Furthermore, the Pawley-refined PXRD profiles match the experimental PXRD patterns very well with  $R_{wp}$  of 2.73% and  $R_p$  of 2.09% (Fig. 2a). However, the calculated PXRD pattern for the staggered structure does not agree with the experimental PXRD patterns (Fig. 2c and e), thus we exclude the possibility of the staggered stacking mode in the Py-TPE-COF.

The permanent porosity of the Py-TPE-COF is investigated by nitrogen sorption measurements at 77 K, after being activated by degassing the COF sample at 120 °C for 8 h (Fig. 3a). The Brunauer–Emmett–Teller (BET) surface area and pore volume

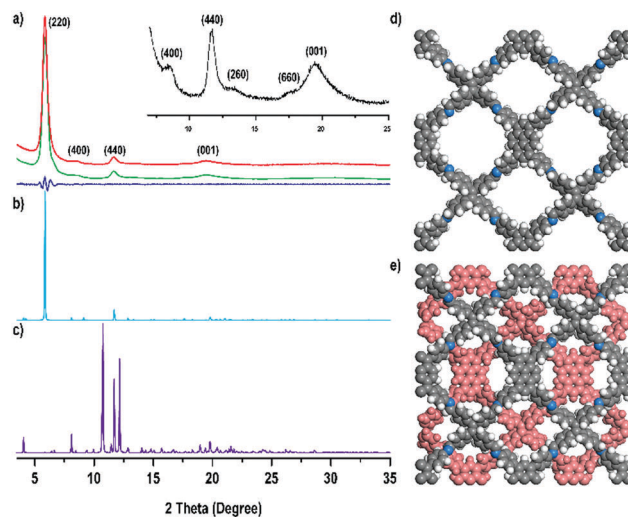


Fig. 2 Powder XRD patterns of (a) experimental (red), Pawley-refined (green), difference between the experimental and refined PXRD patterns (dark blue). Simulated powder XRD patterns for (b) eclipsed structure, (c) staggered structure. Simulated crystal structures of (d) eclipsed structure, (e) staggered structure, views from the  $c$  axis. C, gray; H, white; N, blue; lower layer, red.

are calculated to be  $987 \text{ m}^2 \text{ g}^{-1}$  and  $0.77 \text{ cm}^3 \text{ g}^{-1}$  ( $P/P_0 = 0.983$ ), respectively. The pore-size distribution is calculated based on nonlocal density functional theory (NLDFT), resulting in a micropore size centered at 1.1 nm (Fig. 3a, inset), which shows good agreement with the pore size predicted from the crystal structure of the Py-TPE-COF (1.2 nm). The morphology of the Py-TPE-COF is revealed by scanning electron microscopy (SEM) to be spherical (Fig. 3b and Fig. S24, ESI<sup>†</sup>). Transmission electron microscopy (TEM) images of the Py-TPE-COF also reveal that the COF crystallizes in the form of sphere-like nanoparticles with domain sizes of 300–500 nm (Fig. 3c and Fig. S25, ESI<sup>†</sup>), this observation is consistent with the nanoparticle size shown in the SEM characterization.

To our delight, Py-TPE-COF nanoparticles, which are dispersed well in tetrahydrofuran (THF), display a bright blue photoluminescence (PL) which is visible with the naked eye when excited by 365 nm ultraviolet lamps (Fig. 4a, inset c; and Fig. S14, ESI<sup>†</sup>). This directly confirms the highly fluorescence emission of Py-TPE-COF nanoparticles dispersed in organic solvents. UV-Vis spectra show that the model compounds (TPE-M and Py-M) exhibit absorption peaks at 363 nm and 401 nm, respectively, whereas the Py-TPE-COF exhibits an absorption peak centered at 401 nm (Fig. S18, ESI<sup>†</sup>). Under 365 nm light, a suspension of Py-TPE-COF dispersed in THF, acetone, acetonitrile (ACN) and dimethylformamide (DMF) emits either bright blue or blue-green luminescence with PL bands centered at 462, 469, 474 and 493 nm, respectively (Fig. S20 and S15, ESI<sup>†</sup>). The red-shifted emission band (from 462 to 493 nm) indicates the presence of the dipolar effect of solvents in fluorescence.<sup>9</sup> Model compounds (including Py-M and TPE-M) and reference imine-based COFs<sup>7b,e,d</sup> (including Py-COF and TPE-COF, ESI<sup>†</sup>) show none or very weak fluorescence emission (Fig. 4a, inset c–g and Fig. S14, S16, ESI<sup>†</sup>). The poor PL of model compound Py-M indicates the effect of

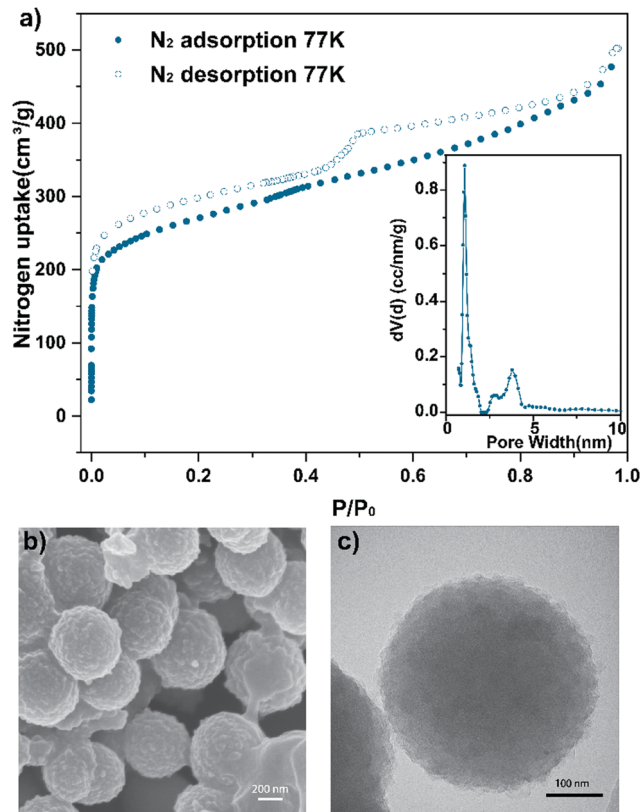


Fig. 3 (a) Nitrogen sorption isotherms of the Py-TPE-COF, the  $N_2$  adsorption isotherm at 77 K, adsorption ( $\bullet$ ) and desorption ( $\circ$ ), (inset) pore size distribution by NLDFT, (b) the SEM image of Py-TPE-COF nanoparticles, (c) TEM image of Py-TPE-COF nanoparticles.

imine linkage in PL quenching. Furthermore, the absolute photoluminescence quantum yields (PLQY) of model compounds and imine-based COFs are investigated using integrating sphere methods (Fig. 4a). The absolute PLQY of the Py-TPE-COF ranges from 13.7% to 21.1% in various organic solvents,<sup>10</sup> whereas the model compounds exhibit absolute PLQY less than 0.1% (Fig. 4a). The dramatic difference between the Py-TPE-COF and model compounds indicates that the non-planar TPE structure introduced into the COF structure can overcome the aggregation caused quenching (ACQ) process and enhance the PL. The PLQY of two reference frameworks, the Py-COF and TPE-COF, with planar building units are observed to be 0.3% and <0.1% (Fig. 4a), thus underscoring the importance of having non-planar building units for avoiding quenching. According to the theoretically simulated crystal structure of the Py-COF<sup>7e</sup> and Py-TPE-COF, the  $\pi$ - $\pi$  stacking distances are calculated to be 3.90 Å and 4.04 Å, respectively, thus the enlarged interlayer distance of the Py-TPE-COF due to the presence of non-planar units weakens the  $\pi$ - $\pi$  interactions. Although the reduction of  $\pi$ - $\pi$  interactions may mitigate the effects of ACQ in PL quenching,<sup>11</sup> we found that the highest PLQY was obtained from the Py-TPE-COF which had been transformed into spherical sub-micron nanoparticles. Due to the surface curvature in these nanoparticles, the skeleton and linkages in the COF are strained, thus the imine bond rotation may be restricted, which removes the non-radiative pathway. To the best of our knowledge,

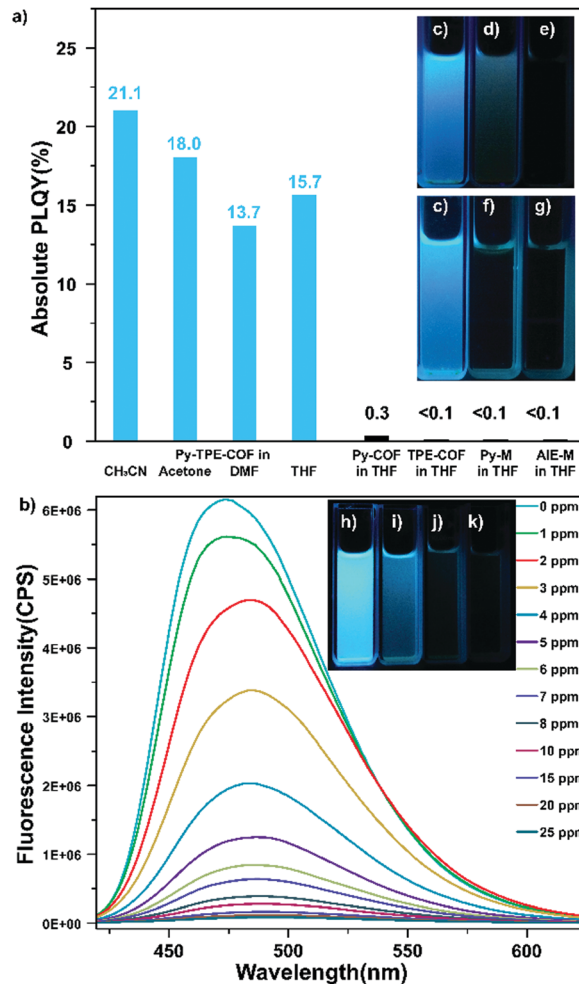


Fig. 4 (a) Absolute fluorescence quantum yield of the Py-TPE-COF dispersed in acetonitrile, acetone, DMF, THF and the Py-COF, the TPE-COF with model compounds Py-M and TPE-M dispersed in THF. (inset) The fluorescence images of (c) Py-TPE-COF (d) Py-COF (e) TPE-COF (f) Py-M and (g) TPE-M dispersed in THF, under 365 nm illumination. (b) Fluorescence quenching experiments of the Py-TPE-COF upon addition of TNP (0–25 ppm) in acetone, (inset) the fluorescence image of (h) 0 ppm (i) 3 ppm (j) 6 ppm (k) 9 ppm TNP in the COF solution.

our Py-TPE-COF nanoparticles exhibit the highest PLQY of the imine-based COFs reported to date.

Taking advantage of their high fluorescence and porosity, Py-TPE-COF nanoparticles can be exploited as highly sensitive fluorescence sensors for the detection of explosives, which is based on the principle of charge transfer induced fluorescence quenching.<sup>12</sup> To demonstrate the chemical sensing capability, 2,4,6-trinitrophenol (TNP) is chosen as the model compound. Fluorescence quenching experiments are investigated in an acetone solvent, because of better dispersion of the Py-TPE-COF and TNP solubility in acetone (Fig. 4b). With merely 1 ppm concentration of TNP being added, the PL intensity of the Py-TPE-COF decreases sharply. The PL intensity decreases monotonically with the addition of TNP, the quenching percentage increases to 95.5% when the concentration of TNP is 10 ppm. To demonstrate the detection selectivity of the Py-TPE-COF, other non-explosive molecular

analogs with similar structures, including 2,4-dinitrophenol (DNP), 2,4-dinitrotoluene (DNT), 2-nitrotoluene (NT) and 2-nitrophenol (NP), are tested. Upon the addition of 10 ppm of these molecular analogs to Py-TPE-COF suspensions under the same conditions, there are only small to marginal decrease in the PL intensities for DNP (15.6%), DNT (0.8%), NT (1.7%) and NP (1.3%) (Fig. S23, ESI<sup>†</sup>), which prove the excellent target selectivity of TNP. The hydroxy group of TNP may form a hydrogen bond with the open nitrogen atoms in the imine Py-TPE-COF on the pore walls. The complexation of TNP with the Py-TPE-COF results in a non-emissive complex that traps the excitation energy of the COF skeletons, resulting in static fluorescence quenching.

In summary, we have explored a new strategy to construct a 2D highly photoluminescent imine-based COF using  $C_2$  symmetric building blocks that are connected through [4+4] imine condensation. The Py-TPE-COF is a blue fluorescent imine-based COF with the highest reported PLQY (up to 21.1%) to date. We suggest two reasons for the non-quenched photoluminescence in our COF. Firstly, the use of non-planar building blocks reduces  $\pi$ - $\pi$  interactions. Secondly, engineering COFs into spherical nanoparticles creates curvature-induced strain, which may restrict bond rotations in imine linkages and reduce  $\pi$ - $\pi$  stacking. These factors overcome the ACQ mechanism of the pyrene building units. A combined strategy for using non-planar molecular building blocks and morphology engineering of the COF should be amenable to a diverse range of synthetic design, thus opening routes to the synthesis of COF materials with high fluorescence quantum yields.

The authors acknowledge the NRF-CRP grant "Two Dimensional Covalent Organic Framework: Synthesis and Applications". Grant number NRF-CRP16-2015-02, funded by the National Research Foundation, Prime Minister's Office, Singapore. This project is also supported by Shenzhen Peacock Plan (Grant No. KQTD2016053112042971).

## Conflicts of interest

There are no conflicts to declare.

## Notes and references

- 1 (a) C. S. Diercks and O. M. Yaghi, *Science*, 2017, **355**, 923; (b) P. J. Waller, F. Gándara and O. M. Yaghi, *Acc. Chem. Res.*, 2015, **48**, 3053.

- 2 (a) Y. Zeng, R. Zou and Y. Zhao, *Adv. Mater.*, 2016, **28**, 2855; (b) C. J. Doonan, D. J. Tranchemontagne, T. G. Glover, J. R. Hunt and O. M. Yaghi, *Nat. Chem.*, 2010, **2**, 23547; (c) H. Furukawa and O. M. Yaghi, *J. Am. Chem. Soc.*, 2009, **131**, 8875; (d) Q. Gao, L. Bai, X. Zhang, P. Wang, P. Li, Y. Zeng, R. Zou and Y. Zhao, *Chin. J. Chem.*, 2015, **33**, 90.
- 3 (a) S.-Y. Ding, J. Gao, Q. Wang, Y. Zhang, W.-G. Song, C.-Y. Su and W. Wang, *J. Am. Chem. Soc.*, 2011, **133**, 19816; (b) S. Lin, C. S. Diercks, Y.-B. Zhang, N. Kornienko, E. M. Nichols, Y. Zhao, A. R. Paris, D. Kim, P. Yang, O. M. Yaghi and C. J. Chang, *Science*, 2015, **349**, 1208; (c) H. Xu, J. Gao and D. Jiang, *Nat. Chem.*, 2015, **7**, 905.
- 4 (a) S. Dalapati, S. Jin, J. Gao, Y. Xu, A. Nagai and D. Jiang, *J. Am. Chem. Soc.*, 2013, **135**, 17310; (b) S. Dalapati, E. Jin, M. Addicoat, T. Heine and D. Jiang, *J. Am. Chem. Soc.*, 2016, **138**, 5797; (c) S.-Y. Ding, M. Dong, Y.-W. Wang, Y.-T. Chen, H.-Z. Wang, C.-Y. Su and W. Wang, *J. Am. Chem. Soc.*, 2016, **138**, 3031.
- 5 Q. Fang, J. Wang, S. Gu, R. B. Kaspar, Z. Zhuang, J. Zheng, H. Guo, S. Qiu and Y. Yan, *J. Am. Chem. Soc.*, 2015, **137**, 8352.
- 6 (a) C. R. DeBlase, K. E. Silberstein, T.-T. Truong, H. D. Abruña and W. R. Dichtel, *J. Am. Chem. Soc.*, 2015, **135**, 16821; (b) W. Liu, X. Luo, Y. Bao, Y. P. Liu, G.-H. Ning, I. Abdelwahab, L. Li, C. T. Nai, Z. G. Hu, D. Zhao, B. Liu, S. Y. Quek and K. P. Loh, *Nat. Chem.*, 2017, **9**, 563; (c) E. Jin, M. Asada, Q. Xu, S. Dalapati, M. A. Addicoat, M. A. Brady, H. Xu, T. Nakamura, T. Heine, Q. Chen and D. Jiang, *Science*, 2017, **357**, 673; (d) C. Montoro, D. Rodríguez-San-Miguel, E. Polo, R. Escudero-Cid, M. L. Ruiz-González, J. A. R. Navarro, P. Ocón and F. Zamora, *J. Am. Chem. Soc.*, 2017, **139**, 10079.
- 7 (a) M. G. Rabbani, A. K. Sekizkardes, Z. Kahveci, T. E. Reich, R. Ding and H. M. El-Kaderi, *Chem. – Eur. J.*, 2013, **19**, 3324; (b) T.-Y. Zhou, S.-Q. Xu, Q. Wen, Z.-F. Pang and X. Zhao, *J. Am. Chem. Soc.*, 2014, **136**, 15885; (c) Z.-F. Pang, S.-Q. Xu, T.-Y. Zhou, R.-R. Liang, T.-G. Zhan and X. Zhao, *J. Am. Chem. Soc.*, 2016, **138**, 4710; (d) L. Ascherl, T. Sick, J. T. Margraf, S. H. Lapidus, M. Calik, C. Hettstedt, K. Karaghiosoff, M. Döblinger, T. Clark, K. W. Chapman, F. Auras and T. Bein, *Nat. Chem.*, 2016, **8**, 310; (e) S. Reuter, D. Bessinger, M. Döblinger, C. Hettstedt, K. Karaghiosoff, S. Herbert, P. Knochel, T. Clark and T. Bein, *J. Am. Chem. Soc.*, 2016, **138**, 16703; (f) X. Chen, N. Huang, J. Gao, H. Xu, F. Xu and D. Jiang, *Chem. Commun.*, 2014, **50**, 6161.
- 8 P. J. Waller, S. J. Lyle, T. M. O. Popp, C. S. Diercks, J. A. Reimer and O. M. Yaghi, *J. Am. Chem. Soc.*, 2016, **138**, 15519.
- 9 (a) J. R. Lakowicz, *Principles of Fluorescence Spectroscopy*, Springer, New York, 3rd edn, 2006; (b) K. Kalyanasundaram and J. K. Thomas, *J. Am. Chem. Soc.*, 1977, **99**, 2039.
- 10 (a) W. H. Melhuish, *J. Phys. Chem.*, 1961, **65**, 229; (b) D. Magde, R. Wong and P. G. Seybold, *Photochem. Photobiol.*, 2002, **75**, 327.
- 11 (a) C. A. Hunter and J. K. M. Sanders, *J. Am. Chem. Soc.*, 1990, **112**, 5525; (b) E. A. M. Dipl-Chem, R. K. Castellano and F. Diederich, *Angew. Chem., Int. Ed.*, 2003, **42**, 1210; (c) C. R. Martinez and B. L. Iverson, *Chem. Sci.*, 2012, **3**, 2191.
- 12 Z. Wei, Z.-Y. Gu, R. K. Arvapally, Y.-P. Chen, R. N. McDougald, Jr, J. F. Ivy, A. A. Yakovenko, D. Feng, M. A. Omary and H.-C. Zhou, *J. Am. Chem. Soc.*, 2014, **136**, 8269.